

Quasiparticle interference testing the possible pairing symmetry in Sr_2RuO_4

Cong-Cong Zhang(张聪聪), Jin-Hua Sun(孙金华), Yang-Yang(杨阳), Wan-Sheng Wang(王万胜)

Citation: Chin. Phys. B . 2020, 29(6): 067401 . **doi:** 10.1088/1674-1056/ab8888
Journal homepage: http://cpb.iphy.ac.cn; http://iopscience.iop.org/cpb

What follows is a list of articles you may be interested in

Unconventional chiral d-wave superconducting state in strained graphene

Feng Xu(徐峰), Lei Zhang(张磊)

Chin. Phys. B . 2019, 28(11): 117403 . **doi:** 10.1088/1674-1056/ab478c

Josephson effect in the strontium titanate/lanthanum aluminate junction

Xing Yang(阳星), Jie Chen(陈杰), Yabin Yu(余亚斌), Quanhui Liu(刘全慧)

Chin. Phys. B . 2019, 28(9): 097401 . **doi:** 10.1088/1674-1056/ab33f4

Topological phase diagrams and Majorana zero modes of the Kitaev ladder and tube

Yiming Wang(王一鸣), Zhidan Li(李志聃), Qiang Han(韩强)

Chin. Phys. B . 2018, 27(4): 047401 . **doi:** 10.1088/1674-1056/27/4/047401

Comparison of band structure and superconductivity in $FeSe_{0.5}Te_{0.5}$ and FeS

Yang Yang(杨阳), Shi-Quan Feng(冯世全), Yuan-Yuan Xiang(向圆圆), Hong-Yan Lu(路洪艳), Wan-Sheng Wang(王万胜)

Chin. Phys. B . 2017, 26(12): 127401 . **doi:** 10.1088/1674-1056/26/12/127401

Topological phase transition in a ladder of the dimerized Kitaev superconductor chains

Bo-Zhen Zhou(周博臻), Bin Zhou(周斌)

Chin. Phys. B . 2016, 25(10): 107401 . **doi:** 10.1088/1674-1056/25/10/107401

Quasiparticle interference testing the possible pairing symmetry in Sr_2RuO_4*

Cong-Cong Zhang(张聪聪)[1], Jin-Hua Sun(孙金华)[1], Yang Yang(杨阳)[2], and Wan-Sheng Wang(王万胜)[1,3,†]

[1] *Department of Physics, Ningbo University, Ningbo* 315211, *China*
[2] *College of Physics and Electronic Engineering, Zhengzhou University of Light Industry, Zhengzhou* 450002, *China*
[3] *School of Engineering, Lishui University, Lishui* 323000, *China*

(Received 27 December 2019; revised manuscript received 19 March 2020; accepted manuscript online 12 April 2020)

The quasiparticle interference (QPI) patterns of the superconducting state in Sr_2RuO_4 are theoretically studied by taking into account the spin–orbital coupling and two different pairing modes, chiral p-wave pairing and equal d-wave pairing, in order to propose an experimental method to test them. Both of the QPI spectra for the two pairing modes have clearly peaks evolving with energy, and their locations can be determined from the tips of the constant energy contour. But the number, location, and evolution of these peaks with energy are different between the two pairing modes. The different behaviors of the QPI patterns in these two pairing modes may help to resolve whether Sr_2RuO_4 is a chiral p-wave or d-wave superconductor.

Keywords: Sr_2RuO_4, quasiparticle interference, chiral p-wave, d-wave

PACS: 74.20.–z, 74.20.Rp, 74.70.–b **DOI:** 10.1088/1674-1056/ab8888

1. Introduction

The layered perovskite ruthenate Sr_2RuO_4 has long been the focus of intense research because it is one of the rare candidates of topological superconductors. Early measurements of nuclear magnetic resonance (NMR)[1–4] and spin polarized neutron scattering[5] show an absence of drop in the spin susceptibility across T_c, providing identification of spin-triplet pairing in Sr_2RuO_4. μSR[6] and the polar Kerr effect[7] reveal that the time reversal (TR) symmetry is spontaneously broken below T_c, suggesting chiral p-wave triplet pairing. The d-vector of the triplet pairing is proposed as $\hat{z}(k_x \pm ik_y)$,[8,9] which is analogous to that in the superfluid ^{3}He-A phase.[10] On the other hand, abundant of low-energy quasiparticle excitations are observed in specific heat,[11–13] superfluid density,[14] the spin-lattice relaxation rate,[15] thermal conductivity,[16–18] and ultrasound attenuation[19] deep in the superconducting (SC) state, indicating gap nodes on the Fermi surface (FS) (forming nodal lines along the direction perpendicular to the RuO_2 plane). To explain the nodal-like behavior, a simple scenario is to assume symmetry protected d-wave pairing.

However, the scenario of d-wave pairing is inconsistent with the signatures of the chiral p-wave triplet. An alternative scenario is that the chiral p-wave gap function may have deep minima or accidental nodes.[20–27] Recently, functional renormalization group (FRG) study of Sr_2RuO_4 with spin–orbital coupling (SOC) finds that the pairing symmetry of Sr_2RuO_4 is chiral p-wave, but the atomic SOC induces near nodes for quasiparticle excitations, which explains the experimental puzzle between the d-wave-like feature observed in thermal experiments and the chiral p-wave triplet pairing revealed in NMR and Kerr effect.[28] But, very recently, in-plane ^{17}O NMR measurements reveal a very substantial drop of the Knight shift below T_c,[29,30] and current-field inversion experiments using Josephson tunnel junctions indicate that the TR symmetry is preserved in Sr_2RuO_4.[31] Those phenomena are in sharp contradistinction to the early NMR and Kerr effect experiments. Therefore, extensive reassessment of the pairing symmetry of Sr_2RuO_4 has quickly materialized.

The scanning tunneling microscopy (STM) technique is a powerful method to determine the pairing symmetry of unconventional superconductors. The determination of the tunneling conductance map on a finite surface area leads, via Fourier transformation, to the quasiparticle interference (QPI) pattern that is caused by impurity scattering on the surface. This pattern contains information on the normal-state conduction band FS as well as on the pairing gaps of the SC state.[32–34] Early theoretical studies of QPI patterns of the SC state in Sr_2RuO_4 find clear QPI peaks evolving with energy for chiral p-wave pairing state based on the model without SOC.[35,36] However, angular-resolved photo-emission spectroscopy (ARPES) measurements[37–42] and FRG study[28] show that SOC plays an important role in the properties of the SC state in Sr_2RuO_4. Thus, we may need to reconsider the QPI patterns of Sr_2RuO_4 with the effect of SOC.

In this paper, we therefore investigate the expected QPI structure of Sr_2RuO_4 with SOC and two possible pairing modes, chiral p-wave pairing and equal d-wave pair-

*Project supported by the National Natural Science Foundataion of China (Grant Nos. 11604168, 11604166, and 11604303). WSW also acknowledges the supports by K. C. Wong Magna Fund in Ningbo University.

†Corresponding author. E-mail: wangwansheng@nbu.edu.cn

© 2020 Chinese Physical Society and IOP Publishing Ltd

ing proposed by FRG calculations[28] and thermal conductivity experiments,[18] respectively, to propose an experimental method to test them. We find that the QPI spectra have clearly peaks evolving with energy for both of the two pairing modes. But there are five main peaks for chiral p-wave pairing and six main peaks for equal d-wave pairing, and the location and evolution of those peaks with energy are different between the two pairing modes. These features, if compared to experimental determination of QPI, may be used to further quantify the pairing symmetry of Sr_2RuO_4.

2. Model and method

We start with the three-orbital model with the effect of SOC proposed in Ref. [41]. The normal state part of the Hamiltonian can be written as

$$\begin{aligned} H_0 &= \sum_{\boldsymbol{k}} \psi^\dagger_{\boldsymbol{k}} h_{\boldsymbol{k}} \psi_{\boldsymbol{k}}, \\ h_{\boldsymbol{k}} &= \epsilon_{\boldsymbol{k}} \sigma_0 - \lambda \boldsymbol{L}\cdot\boldsymbol{\sigma}/2. \end{aligned} \tag{1}$$

Here, $\psi_{\boldsymbol{k}} = (c_{\boldsymbol{k}1\uparrow}, c_{\boldsymbol{k}2\uparrow}, c_{\boldsymbol{k}3\uparrow}, c_{\boldsymbol{k}1\downarrow}, c_{\boldsymbol{k}2\downarrow}, c_{\boldsymbol{k}3\downarrow})^{\mathrm{T}}$ is the fermion spinor, with $c_{\boldsymbol{k}as}$ annihilating an electron of momentum $\boldsymbol{k}$ and spin $s \in (\uparrow,\downarrow)$ on orbital $a \in (1,2,3) \leftrightarrow (\mathrm{d}_{xz}, \mathrm{d}_{yz}, \mathrm{d}_{xy})$. The nonzero elements of the spin-invariant part $\epsilon_{\boldsymbol{k}}$ are (in the orbital basis)

$$\begin{aligned} \epsilon_{11}(\boldsymbol{k}) &= -2(t_1\cos k_x + t_2 \cos k_y) - \mu, \\ \epsilon_{22}(\boldsymbol{k}) &= -2(t_2\cos k_x + t_1 \cos k_y) - \mu, \\ \epsilon_{33}(\boldsymbol{k}) &= -2t_3(\cos k_x + \cos k_y) - 4t_4 \cos k_x \cos k_y \\ &\quad -2t_5(\cos 2k_x + \cos 2k_y) - \mu, \\ \epsilon_{12}(\boldsymbol{k}) &= \epsilon_{21}(\boldsymbol{k}) = -4t_6 \sin k_x \sin k_y, \end{aligned} \tag{2}$$

where μ is the chemical potential. The parameter λ in $h_{\boldsymbol{k}}$ is the SOC, $\boldsymbol{L} = (L^x, L^y, L^z)$ is the orbital angular momentum operator, with

$$\begin{aligned} L^x_{ab} &= 2\mathrm{i}(\delta_{a3}\delta_{b1} - \delta_{a1}\delta_{b3}), \\ L^y_{ab} &= 2\mathrm{i}(\delta_{a2}\delta_{b3} - \delta_{a3}\delta_{b2}), \\ L^z_{ab} &= 2\mathrm{i}(\delta_{a1}\delta_{b2} - \delta_{a2}\delta_{b1}), \end{aligned} \tag{3}$$

and $\boldsymbol{\sigma}/2$ is the spin angular momentum. The parameters that best fit the ARPES experiment of Sr_2RuO_4 are $(t_1, t_2, t_3, t_4, t_5, t_6, \lambda, \mu) = (0.145, 0.016, 0.081, 0.039, 0.005, 0.000, 0.032, 0.122)$ eV.[41] TR and inversion symmetries dictate Kramers degeneracy in the eigenstates of $h_{\boldsymbol{k}}$, which in our case can be written in the form

$$|\boldsymbol{k}n+\rangle = (u_{\boldsymbol{k}n}, v_{\boldsymbol{k}n}, 0, 0, 0, w_{\boldsymbol{k}n})^{\mathrm{T}}, \quad |\boldsymbol{k}n-\rangle = T|\boldsymbol{k}n+\rangle, \tag{4}$$

where $n \in (\alpha, \beta, \gamma)$ labels the band, $\nu = \pm$ the pseudo-spin, and $T = \mathrm{i}\sigma_y K$ is the TR operator. Notice spin SU(2) is violated by SOC, so singlet and triplet pairings can mix.

The total Hamiltonian for the SC state can be written as

$$\begin{aligned} H &= \frac{1}{2}\sum_{\boldsymbol{k}} \Psi^\dagger_{\boldsymbol{k}} M_{\boldsymbol{k}} \Psi_{\boldsymbol{k}}, \\ \Psi^\dagger_{\boldsymbol{k}} &= (\psi^\dagger_{\boldsymbol{k}}, \psi^t_{-\boldsymbol{k}}), \end{aligned}$$

$$M_{\boldsymbol{k}} = \begin{pmatrix} h_{\boldsymbol{k}} & \Delta_{\boldsymbol{k}} \\ \Delta^\dagger_{\boldsymbol{k}} & -h^t_{-\boldsymbol{k}} \end{pmatrix}. \tag{5}$$

For the chiral p-wave pairing proposed in Ref. [28], we have

$$\begin{aligned} \Delta_{\boldsymbol{k}} &= \Delta_p[P_x(\boldsymbol{k}) \pm \mathrm{i}P_y(\boldsymbol{k})]\mathrm{i}\sigma_y, \\ P_x(\boldsymbol{k}) &= \begin{pmatrix} -p_6\sigma_z & \mathrm{i}p_5\sigma_0 & p_3\sigma_y \\ -\mathrm{i}p_5\sigma_0 & p_6\sigma_z & p_4\sigma_x \\ p_3\sigma_y & p_4\sigma_x & (p_1 + p_2\cos k_y)\sigma_z \end{pmatrix} \sin k_x, \\ P_y(\boldsymbol{k}) &= \begin{pmatrix} p_6\sigma_z & \mathrm{i}p_5\sigma_0 & p_4\sigma_y \\ -\mathrm{i}p_5\sigma_0 & -p_6\sigma_z & p_3\sigma_x \\ p_4\sigma_y & p_3\sigma_x & (p_1 + p_2\cos k_x)\sigma_z \end{pmatrix} \sin k_y, \end{aligned}$$

where σ are the Pauli matrices acting on the spin bases. Each p_i-complex transforms as $p_{x/y}$ in $P_{x/y}$ under combined symmetry operations on (spin, orbital, lattice). The σ_0-part is the spin singlet and the $\sigma_{x/y/z}$-parts are triplets. The relative ratio between the coefficients $p_{1,\ldots,6}$ is given by

$$(p_2, p_3, p_4, p_5, p_6) \cong (-0.8, 0.33, 0.08, 0.04, -0.02)p_1.$$

To clear see the gap structure on the Fermi surface, we project the pairing matrix onto the normal state band basis as, with pseudo-spin $\nu = \pm$ and band label $n \in (\alpha, \beta, \gamma)$,

$$\begin{aligned} \Delta^{\nu\nu'}_{nn'}(\boldsymbol{k}) &= \langle \boldsymbol{k}n\nu|[P_x(\boldsymbol{k}) + \mathrm{i}P_y(\boldsymbol{k})]T|-\boldsymbol{k}n'\nu'\rangle \\ &= -\langle \boldsymbol{k}n\nu|[P_x(\boldsymbol{k}) + \mathrm{i}P_y(\boldsymbol{k})]|\boldsymbol{k}n'\nu'\rangle, \end{aligned} \tag{6}$$

we have applied $|-\boldsymbol{k}n\nu\rangle = T|\boldsymbol{k}n\nu\rangle$ in the second line. We find that in our case $\Delta^{\nu\nu}_{nn}(\boldsymbol{k}) = \nu\Delta_n(\boldsymbol{k})$, $\Delta^{\nu\neq\nu'}_{nn}(\boldsymbol{k}) = 0$, and the inter-band part $\Delta^{\nu\nu'}_{n\neq n'}(\boldsymbol{k}) \to 0$. (The inter-band pairing is unimportant since T_c is low and the three bands are nondegenerate at the same momentum.) Figure 1(a) shows the resulting gap structure $|\Delta_n(\boldsymbol{k})|$ (normalized by the maximum gap Δ_0 on the γ pocket) on the FS, we can clear see two sets of near nodes along Γ–X and Γ–M directions on the γ pocket, and one set of gap minimum along M–X (Γ–X) direction on the α (β) pocket.

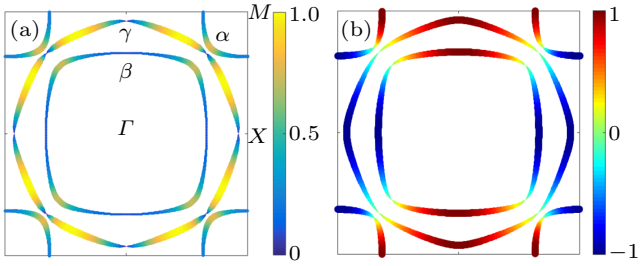


Fig. 1. The gap structure on the Fermi surface in the Brillouin zone, (a) $|\Delta_n(\boldsymbol{k})|$ of chiral p-wave pairing and (b) $\Delta^{++}_n(\boldsymbol{k})$ of equal d-wave pairing. Both are normalized by the maximum gap Δ_0, and their magnitude is roughly reflected by the linewidth.

For equal d-wave pairing suggested by Ref. [18], the pairing matrix in the band basis with pseudo-spin is given by

$$\Delta^{++}_n(\boldsymbol{k}) = \Delta^{--}_n(\boldsymbol{k}) = \Delta_{\mathrm{d}n}(\cos k_x - \cos k_y), \tag{7}$$

with the relative ratio of $\Delta_{\mathrm{d}n}$ as $(\Delta_{\mathrm{d}\alpha} : \Delta_{\mathrm{d}\beta} : \Delta_{\mathrm{d}\gamma}) = (1.67 : 0.671 : 0.5068)$ to make sure the maximum gap Δ_0 on each band be equal. Figure 1(b) shows the corresponding $\Delta^{++}_n(\boldsymbol{k})$

(normalized by Δ_0) on the Fermi surface. In both models, we set the maximum gap $\Delta_0 = 0.004$ eV.

When a single impurity is located at the origin, the impurity Hamiltonian can be written as

$$\begin{aligned} H_{\rm imp} &= V_{\rm s} \sum_{a=1}^{3} \sum_{\sigma=\uparrow,\downarrow} c^{\dagger}_{0a\sigma} c_{0a\sigma} \\ &= \frac{V_{\rm s}}{N} \sum_{a=1}^{3} \sum_{\sigma=\uparrow,\downarrow} \sum_{\boldsymbol{k},\boldsymbol{k}'} c^{\dagger}_{\boldsymbol{k}a\sigma} c_{\boldsymbol{k}'a\sigma}, \end{aligned} \tag{8}$$

with N being the system size (512×512 throughout the paper). We consider the nonmagnetic impurity only, diagonal in the orbital basis and with a scattering strength $V_{\rm s} = 4\Delta_0$ for definiteness. Following the standard T-matrix procedure,[32] the Green's function matrix is defined as

$$g(\boldsymbol{k},\boldsymbol{k}',\tau) = -\langle T_\tau \Psi_{\boldsymbol{k}}(\tau) \Psi^{\dagger}_{\boldsymbol{k}'}(0)\rangle, \tag{9}$$

and

$$g(\boldsymbol{k},\boldsymbol{k}',\omega) = \delta_{\boldsymbol{k}\boldsymbol{k}'} g_0(\boldsymbol{k},\omega) + g_0(\boldsymbol{k},\omega) T(\omega) g_0(\boldsymbol{k}',\omega). \tag{10}$$

Here $g_0(\boldsymbol{k},\omega)$ is the Green's function in the absence of the impurity

$$\begin{aligned} g_0(\boldsymbol{k},\omega) &= \left[(\omega + {\rm i}0^+) I - M_{\boldsymbol{k}}\right]^{-1}, \\ T(\omega) &= U \left[\boldsymbol{I} - \frac{U}{N} \sum_{\boldsymbol{q}} g_0(\boldsymbol{q},\omega)\right]^{-1}, \end{aligned} \tag{11}$$

where $\boldsymbol{I}$ is a 12×12 unit matrix and

$$U^{nn} = \begin{cases} V_{\rm s}, & n = 1,\ldots,6, \\ -V_{\rm s}, & n = 7,\ldots,12. \end{cases}$$

The experimentally measured LDOS is expressed as

$$\begin{aligned} \rho(\boldsymbol{r},\omega) &= -\frac{1}{\pi} \sum_{a=1}^{3} \sum_{\sigma=\uparrow,\downarrow} {\rm Im} \langle\langle c_{\boldsymbol{r}a\sigma} | c^{\dagger}_{\boldsymbol{r}a\sigma} \rangle\rangle_{\omega+{\rm i}0^+} \\ &= -\frac{1}{N\pi} \sum_{m=1}^{6} \sum_{\boldsymbol{k},\boldsymbol{k}'} {\rm Im} \left[g_{mm}(\boldsymbol{k},\boldsymbol{k}',\omega) {\rm e}^{-{\rm i}(\boldsymbol{k}-\boldsymbol{k}')\cdot\boldsymbol{r}} \right], \end{aligned} \tag{12}$$

and its Fourier transform is defined as $\rho(\boldsymbol{q},\omega) = \sum_{\boldsymbol{r}} \rho(\boldsymbol{r},\omega) {\rm e}^{{\rm i}\boldsymbol{q}\cdot\boldsymbol{r}}$, which can be expressed as

$$\begin{aligned} \rho(\boldsymbol{q},\omega) = -\frac{1}{2\pi} \sum_{m=1}^{6} \sum_{\boldsymbol{k}} & {\rm Im}[g_{mm}(\boldsymbol{k},\boldsymbol{k}+\boldsymbol{q},\omega) + g_{mm}(\boldsymbol{k},\boldsymbol{k}-\boldsymbol{q},\omega)] \\ & + {\rm i}\,{\rm Re}\,[g_{mm}(\boldsymbol{k},\boldsymbol{k}+\boldsymbol{q},\omega) - g_{mm}(\boldsymbol{k},\boldsymbol{k}-\boldsymbol{q},\omega)]. \end{aligned} \tag{13}$$

3. Results

For the chiral p-wave pairing, we plot $|\rho(\boldsymbol{q},\omega)|$ in Fig. 2, and five main scattering wave vectors $\boldsymbol{q}_{1,2,3,4,5}$ can be identified [see the arrows in Figs. 2(a) and 2(g)]. The wave vector $\boldsymbol{q}_1$ is along $q_{x/y} = 0$ directions, $\boldsymbol{q}_{2,3}$ are along $q_x = \pm q_y$ directions, while the directions of $\boldsymbol{q}_{4,5}$ are dependent on the bias ω. With the increase of $|\omega|$, $\boldsymbol{q}_1$ moves away from the origin, $\boldsymbol{q}_{2,3}$ move towards the origin, $\boldsymbol{q}_4$ moves towards the origin with the orientation close to $q_x = \pm q_y$ directions, while $\boldsymbol{q}_5$ moves towards $(\pi,0)/(0,\pi)$.

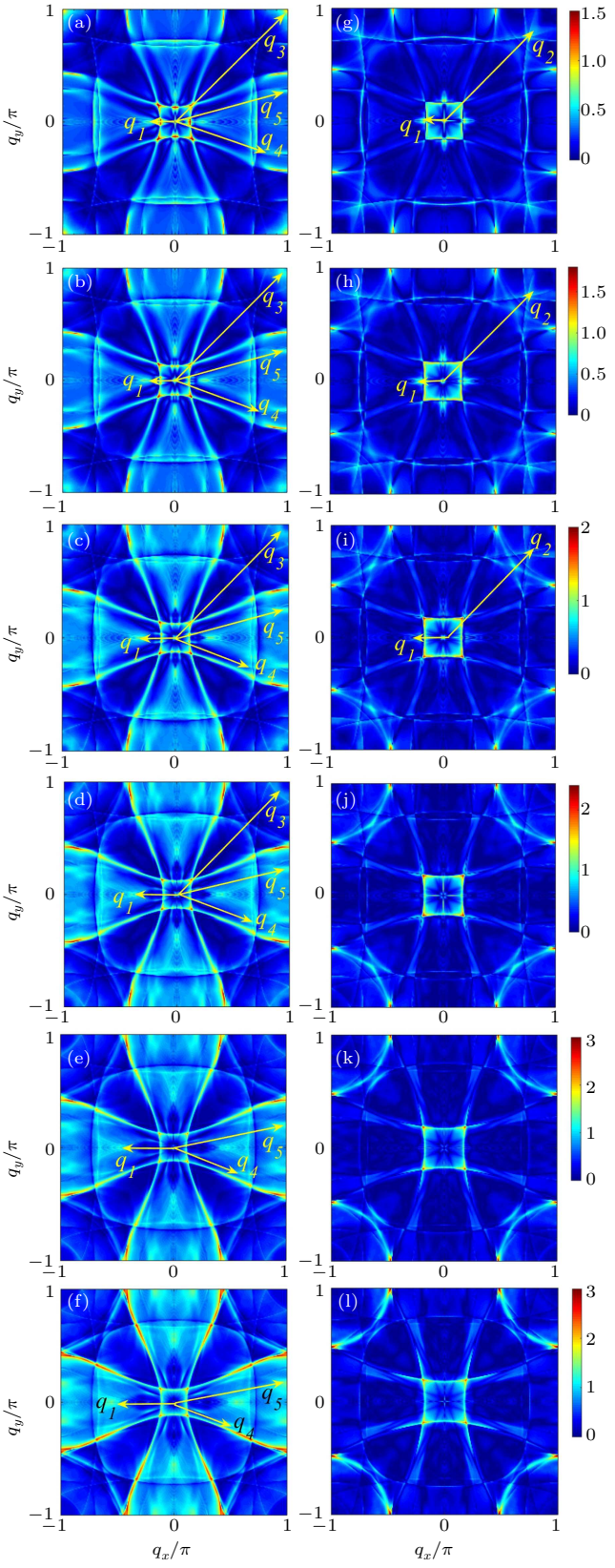


Fig. 2. $|\rho(\boldsymbol{q},\omega)|$ at fixed ω for chiral p-wave pairing state. The point at $\boldsymbol{q} = 0$ is neglected in order to show weak features at other wave vectors. (a)–(f) $\omega/\Delta_0 = 0.3, 0.4, 0.5, 0.6, 0.7, 0.8$; (g)–(l) $\omega/\Delta_0 = -0.3, -0.4, -0.5, -0.6, -0.7, -0.8$. Each row shares the same color scale.

The ω dependence of $\boldsymbol{q}$ can be understood from the evolution of the constant-energy contour (CEC).[32–35] In the

normal state, the CEC of the three bands shows little variation when $|\omega| \leq \Delta_0$ since $\Delta_0 \ll W$, where W is the band width, thus in this energy range $|\rho(\boldsymbol{q},\omega)|$ scarcely evolves with ω. On the contrary, in the SC state, the superconductivity gaps the entire FS with strong anisotropy and leads to complicated structure of deep minima on all of the three Fermi pockets as shown in Fig. 1(a). From Fig. 3 we can find that, around each gap minima, the CEC evolves from a single point at the gap minima to a banana-shaped closed contour at higher energies and the size of the banana increases with $|\omega|$ until its tips trace the normal state FS. By carefully examine the locations of these banana tips, we conclude that the scattering wave vectors $\boldsymbol{q}_{1,2,3,4,5}$ in Fig. 2 should correspond to the wave vectors connecting the banana tips (see the solid arrows in Fig. 3(a)). For example, in Fig. 2(b), at $\omega/\Delta_0 = 0.4$, $\boldsymbol{q}_1/\pi \sim (\pm 0.24, 0)/(0, \pm 0.24)$, $\boldsymbol{q}_3/\pi \sim (\pm 0.96, \pm 0.96)$, $\boldsymbol{q}_4/\pi \sim (\pm 0.71, \pm 0.26)/(\pm 0.26, \pm 0.71)$, and $\boldsymbol{q}_5/\pi \sim (\pm 0.95, \pm 0.26)/(\pm 0.26, \pm 0.95)$. At the same ω, the related CEC tips on γ and α pockets in Fig. 3(a) are located at $(\pm 0.91, \pm 0.12)\pi/(\pm 0.12, \pm 0.91)\pi$ and $(\pm 0.83, \pm 0.64)\pi/(\pm 0.64, \pm 0.83)\pi$, respectively. The derived $\boldsymbol{q}_{1,3,4,5}/\pi$ are $(\pm 0.24, 0)/(0, \pm 0.24)$, $(\pm 1.03, \pm 1.03)$, $(\pm 0.71, \pm 0.27)/(\pm 0.27, \pm 0.71)$, and $(\pm 0.95, \pm 0.27)/(\pm 0.27, \pm 0.95)$, respectively, which agree fairly well with those in Fig. 2(b). Notice that $\boldsymbol{q}_3$ in Fig. 2(b) is located at $(\pm 0.96, \pm 0.96)\pi$ and that derived from Fig. 3(a) is at $(\pm 1.03, \pm 1.03)\pi$, they differ by a reciprocal lattice constant, suggesting that $\boldsymbol{q}_3$ is an umklapp process. As ω/Δ_0 changes from 0.3 to 0.8, the sizes of all bananas increase, thus from Fig. 3(a), $\boldsymbol{q}_1$ should move away from origin, $\boldsymbol{q}_3$ should move toward origin (since it is umklapp process), $\boldsymbol{q}_4$ should be close to origin, and $\boldsymbol{q}_5$ should be close to $(\pi, 0)/(0, \pi)$. As we can see from Figs. 2(a)–2(f), the evolution of $\boldsymbol{q}_{1,3,4,5}$ indeed follows this trend. On the other hand, at $\omega/\Delta_0 = -0.4$, $\boldsymbol{q}_2$ in Fig. 2(h) is located at $(\pm 0.79, \pm 0.79)\pi$ and that derived from Fig. 3(a) is also at $(\pm 0.79, \pm 0.79)\pi$, as $|\omega|$ increases, $|\boldsymbol{q}_2|$ should decrease, as shown in Figs. 2(g)–2(i). We also find that the spectra are asymmetrical with respect to positive and negative ω. Furthermore, $\boldsymbol{q}_2$ and $\boldsymbol{q}_{3,4,5}$ are invisible for positive and negative ω, respectively.

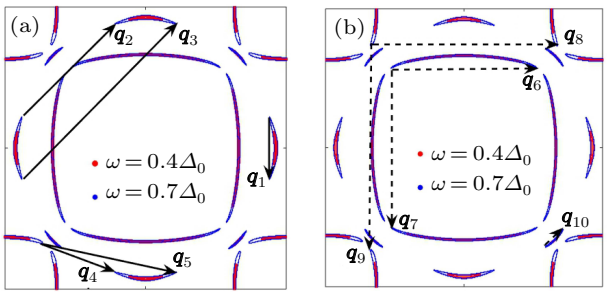


Fig. 3. The CEC of the chiral p-wave pairing state in the Brillouin zone, at $|\omega| = 0.4\Delta_0$ (red) and $|\omega| = 0.7\Delta_0$ (blue). The solid arrows in (a) denote the characteristic scattering wave vectors and dashed arrows in (b) denote the expected scattering wave vectors.

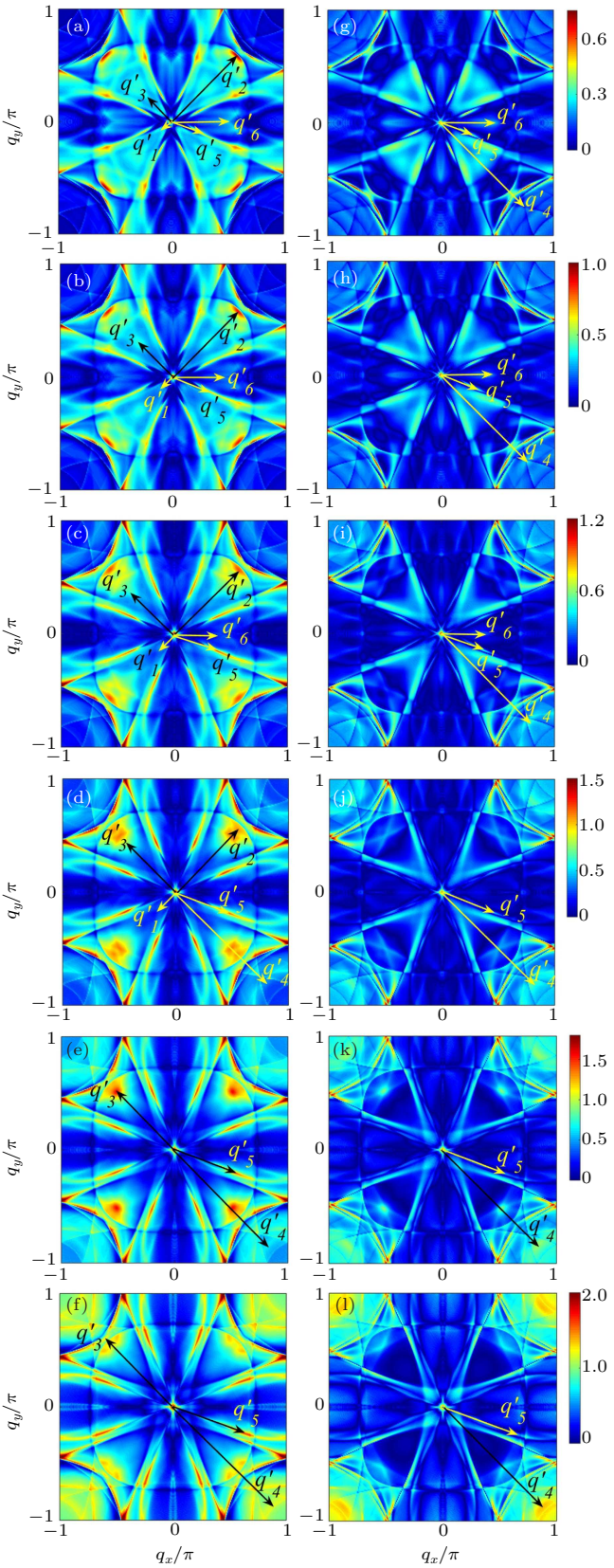


Fig. 4. The same as Fig. 2, but for the equal d-wave pairing.

In addition, apart from the above mentioned $\boldsymbol{q}_{1,2,3,4,5}$, naively we would expect more QPI wave vectors connecting other tips of the CEC. For example, from Fig. 3(b), we can see that there should exist QPI wave vectors like $\boldsymbol{q}_{6,7,8,9,10}$ and others (not shown). However, in Fig. 2 we cannot clearly find

such wave vectors evolving with energy. In order to verify this, we repeated the above calculations for $V_s = 8\Delta_0$ and the results remain qualitatively the same. The reason may be that the intensity of the scattering wave vectors is determined not only by the SC coherence factors,[33] but also by the matrix elements effect of the unitary transformation between the orbital and band bases. In Sr_2RuO_4, all the three bands are coupled by SOC, it is very likely that the matrix elements associated with the above mentioned processes $\boldsymbol{q}_{6,7,8,9,10}$ are vanishingly small, thus those QPI wave vectors cannot be detected experimentally.

For the equal d-wave pairing, different from chiral p-wave pairing discussed above, six main scattering wave vectors $\boldsymbol{q}'_{1,2,3,4,5,6}$ can be identified [see the arrows in Figs. 4(a) and 4(g)]. The wave vectors $\boldsymbol{q}'_{1,2,3,4}$ are along $q_x = \pm q_y$ directions, $\boldsymbol{q}'_6$ is along $q_{x/y} = 0$ directions, while the direction of $\boldsymbol{q}'_5$ is dependent on the bias ω.

As in the chiral p-wave case discussed above, the ω dependence of $\boldsymbol{q}$ can also be understood from the evolution of the CEC. Figure 5 shows the CEC of equal d-wave pairing at $\omega = 0.4\Delta_0$ and $0.7\Delta_0$. By carefully examining the locations of the tip, we can also conclude that the scattering vectors $\boldsymbol{q}'_{1,2,3,4,5,6}$ in Fig. 4 should correspond to the wave vectors connecting the tips. For example, in Fig. 4(b), at $\omega = 0.4\Delta_0$, $\boldsymbol{q}'_1/\pi \sim (\pm 0.10, \pm 0.10)$, $\boldsymbol{q}'_2/\pi \sim (\pm 0.58, \pm 0.58)$, $\boldsymbol{q}'_3/\pi \sim (\pm 0.30, \pm 0.30)$, $\boldsymbol{q}'_5/\pi \sim (\pm 0.11, \pm 0.28)/(\pm 0.28, \pm 0.11)$, and $\boldsymbol{q}'_6/\pi \sim (\pm 0.44, 0)/(0, \pm 0.44)$. At the same ω, the related CEC tips on α and γ pockets in Fig. 5 are located at $(\pm 0.76, \pm 0.66)\pi/(\pm 0.66, \pm 0.76)/\pi$ and $(\pm 0.77, \pm 0.49)\pi/(\pm 0.49, \pm 0.77)\pi$, respectively. The derived $\boldsymbol{q}'_{1,2,3,5,6}/\pi$ are $(\pm 0.10, \pm 0.10)$, $(\pm 1.42, \pm 1.42)$, $(\pm 0.28, \pm 0.28)$, $(\pm 0.11, \pm 0.27)/(\pm 0.27, \pm 0.11)$, and $(\pm 1.54, 0)/(0, \pm 1.54)$, respectively. Agree well with those in Fig. 4(b) with $\boldsymbol{q}'_{2,6}$ being umklapp processes. As ω/Δ_0 changes from 0.3 to 0.8, the sizes of all bananas increase, thus from Fig. 5, $\boldsymbol{q}'_{1,3,5}$ should move away from origin, while $\boldsymbol{q}'_{2,6}$ should move toward origin (since they are umklapp processes). This trend is clearly shown in Figs. 4(a)–4(f). On the other hand, at $\omega = -0.4\Delta_0$, $\boldsymbol{q}'_4$ in Fig. 4(h) is located at $(\pm 0.74, \pm 0.74)\pi$ and that derived from Fig. 5(a) is at $(\pm 1.26, \pm 1.26)\pi$, suggesting that $\boldsymbol{q}'_4$ is an umklapp process, as $|\omega|$ increases, $|\boldsymbol{q}'_4|$ should increase, as shown in Figs. 4(g)–4(l). As in the chiral p-wave pairing, the spectra of d-wave pairing are also asymmetric with respect to positive and negative ω, and some expect QPI wave vectors connecting other tips are unclear, such as $\boldsymbol{q}'_{7,8,9}$ shown by the dashed arrows in Figs. 5(a) and 5(b).

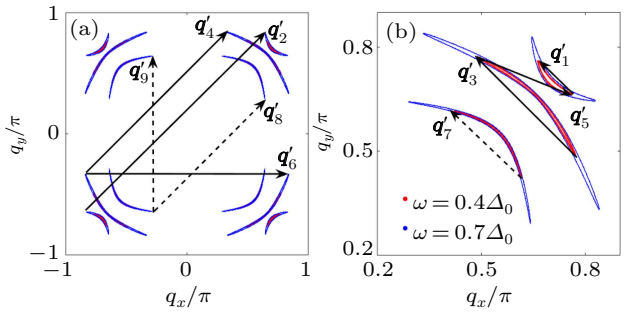


Fig. 5. (a) The CEC of the equal d-wave pairing state, at $|\omega| = 0.3\Delta_0$ (red), $|\omega| = 0.8\Delta_0$ (blue). (b) The same as (a) but around $(q_x, q_y) = (0.6, 0.6)\pi$. The solid (dashed) arrows denote the characteristic (expected) scattering wave vectors.

In Table. 1, the main difference between the chiral p-wave pairing and equal d-wave pairing is summarized.

Table 1. The main difference of the quasiparticle interference patterns between the chiral p-wave pairing and equal d-wave pairing. Notice that each peak includes its symmetric images.

Pairing symmetry	Chiral p-wave	Equal d-wave
Number of peaks	5	6
Location of each peak at $\omega = 0.4\lvert\Delta_0\rvert$ and its evolution with the increase of the bias $\lvert\omega\rvert$. (in units of π)	$(0.24, 0) \to (1, 0)$	$(0.10, 0.10) \to (1, 1)$
	$(0.79, 0.79) \to (0, 0)$	$(0.58, 0.58) \to (0, 0)$
	$(0.96, 0.96) \to (0, 0)$	$(0.30, 0.30) \to (1, 1)$
	$(0.71, 0.26) \to (0, 0)$	$(0.74, 0.74) \to (1, 1)$
	$(0.95, 0.26) \to (1, 0)$	$(0.28, 0.11) \to (1, 0.3)$
		$(0.44, 0) \to (0, 0)$

4. Summary

We have studied the QPI in Sr_2RuO_4 with SOC based on two pairing modes in order to propose an experimental method to test them. Both of the QPI spectra for chiral p-wave pairing and equal d-wave pairing have clear peaks evolving with energy, and their locations can be determined from the tips of the CEC. But the spectra for the two pairing modes are different: (i) for chiral p-wave pairing, there are five main scattering wave vectors, while six main scattering wave vectors can be seen for equal d-wave pairing. (ii) the location and the evolution of those peaks with bias ω are different between the two pairing modes. The main difference between them is summarized in Table. 1. Since the QPI spectrum can be directly measured by STM, the differences of the QPI spectrum between the two pairing modes can used to judge the pairing symmetry for Sr_2RuO_4 and resolve whether Sr_2RuO_4 is a chiral p-wave or d-wave superconductor. In addition, for both models, we repeated the above calculations for $V_s = 8\Delta_0$ and the results remain qualitatively the same, indicating the robustness of the QPI spectra presented in this paper.

References

[1] Ishida K, Mukuda H, Kitaoka Y, Asayama K, Mao Z Q, Mori Y and Maeno Y 1998 *Nature* **396** 658
[2] Murakawa H, Ishida K, Kitagawa K, Mao Z Q and Maeno Y 2004 *Phys. Rev. Lett.* **93** 167004
[3] Ishida K, Manago M, Yamanaka T, Fukazawa H, Mao Z Q, Maeno Y and Miyake K 2015 *Phys. Rev. B* **92** 100502(R)
[4] Manago M, Ishida K, Mao Z Q and Maeno Y 2016 *Phys. Rev. B* **94** 180507(R).
[5] Duffy J A, Hayden S M, Maeno Y, Mao Z Q, Kulda J and McIntyre G J 2000 *Phys. Rev. Lett.* **85** 5412
[6] Luke G M, Fudamoto Y, Kojima K M, Larkin M I, Merrin J, Nachumi B, Uemura Y J, Maeno Y, Mao Z Q, Mori Y Nakamura H and Sigrist M 1998 *Nature* **39** 558
[7] Xia J, Maeno Y, Beyersdorf P T, Fejer M M and Kapitulnik A 2006 *Phys. Rev. Lett.* **97** 167002
[8] Mackenzie A P and Maeno Y,2003 *Rev. Mod. Phys.* **75** 657
[9] Kallin C 2012 *Rep. Prog. Phys.* **75** 042501
[10] Rice T M and Sigrist M 1995 *J. Phys. Condens. Matter* **7** L643
[11] NishiZaki S, Maeno Y and Mao Z Q 1999 *J. Low Temp. Phys.* **117** 1581
[12] Nishizaki S, Maeno Y and Mao Z Q,2000 *J. Phys. Soc. Jpn.* **69** 572
[13] Deguchi K, Mao Z Q, Yaguchi H and Maeno Y 2004 *Phys. Rev. Lett.* **92** 047002
[14] Bonalde I, Yanoff B D, Salamon M B, Van Harlingen D J, Chia E M E, Mao Z Q and Maeno Y 2000 *Phys. Rev. Lett.* **85** 4775
[15] Ishida K, Mukuda H, Kitaoka Y, Mao Z Q, Mori Y and Maeno Y 2000 *Phys. Rev. Lett.* **84** 5387
[16] Suderow H, Brison J P, Flouquet J, Tyler A W and Maeno Y 1998 *J. Phys. Condens. Matter* **10** L597
[17] Suzuki M, Tanatar M A, Kikugawa N, Mao Z Q, Maeno Y and Ishiguro T 2002 *Phys. Rev. Lett.* **88** 227004
[18] Hassinger E, Bourgeois-Hope P, Taniguchi H, René de Cotret S, Grissonnanche G, Anwar M S, Maeno Y, Doiron-Leyraud N and Taillefer L 2017 *Rhys. Rev. X* **7** 011032
[19] Lupien C, MacFarlane W A, Proust C, Taillefer L, Mao Z Q and Maeno Y 2001 *Phys. Rev. Lett.* **86** 5986
[20] Zhitomirsky M E and Rice T M 2001 *Phys. Rev. Lett.* **87** 057001
[21] Nomura T 2005 *J. Phys. Soc. Jpn.* **74** 1818
[22] Raghu S, Kapitulnik A and Kivelson S A 2010 *Phys. Rev. Lett.* **105** 136401
[23] Miyake K and Narikiyo O 1999 *Phys. Rev. Lett.* **83** 1423
[24] Wang Q H, Platt C, Yang Y, Honerkamp C, Zhang F C, Hanke W, Rice T M and Thomale R 2013 *Europhys. Lett.* **104** 17013
[25] Hasegawa Y, Machida K and Ozaki M 2000 *J. Phys. Soc. Jpn.* **69** 336
[26] Graf M J and Balatsky A V 2000 *Phys. Rev. B* **62** 9697
[27] Dahm T, Won H and Maki K 2000 cond-mat/0006301
[28] Wang W S, Zhang C C, Zhang F C and Wang Q H 2019 *Phys. Rev. Lett* **122** 027002
[29] Pustogow A, Luo Y K, Chronister A, Su Y S, Sokolov S, Jerzembeck F, Mackenzie A P, Hicks C W, Nikugawa N, Raghu S, Bauer E D and Brown S E 2019 *Nature* **574** 72
[30] Ishida K, Manago M and Maeno Y 2019 arXiv:1907.12236
[31] Kashiwaya S, Yada K, Tanaka Y, Saitoh K, Kashiwaya H, Koyanagi M, Sato M and Maeno Y 2019 *Phys. Rev. B* **100** 094530
[32] Balatsky A V, Vekhter I and Zhu J X 2006 *Rev. Mod. Phys.* **78** 373
[33] Wang Q H and Lee D H 2003 *Phys. Rev. B* **67** 020511
[34] Hoffman J E, McElroy K, Lee D H, Lang K M, Eisaki H, Uchida S and Davis J C 2002 *Science* **297** 1148
[35] Gao Y, Zhou T, Huang H, Ting C S, Tong P and Wang Q H 2013 *Phys. Rev. B* **88** 094514
[36] Akbari A and Thalmeier P 2013 *Phys. Rev. B* **88** 134519
[37] Damascelli A, Lu D H, Shen K M, Armitage N P, Ronning F, Feng D L, Kim C, Shen Z X, Kimura T, Tokura Y, Mao Z Q and Maeno Y 2000 *Phys. Rev. Lett.* **85** 5194
[38] Haverkort M W, Elfimov I S, Tjeng L H, Sawatzky G A and Damascelli A 2008 *Phys. Rev. Lett.* **101** 026406
[39] Veenstra C N, Zhu Z H, Ludbrook B, Capsoni M, Levy G, Nicolaou A, Rosen J A, Comin R, Kittaka S, Maeno Y, Elfimov I S and Damascelli A 2013 *Phys. Rev. Let.* **110** 097004
[40] Veenstra C N, Zhu Z H, Raichle M, Ludbrook B M, Nicolaou A, Slomski B, Landolt G, Kittaka S, Maeno Y, Dil J H, Elfimov I S, Haverkort M W and Damascelli A 2014 *Phys. Rev. Lett.* **112** 127002
[41] Zabolotnyy V B, Evtushinsky D V, Kordyuk A A, Kim T K, Carleschi E, Doyle B P, Fittipaldi R, Cuoco M, Vecchione A and Borisenko S V 2013 *J. Electron Spectrosc. Relat. Phenom.* **191** 48
[42] Tamai A, Zingl M, Rozbicki E, Cappelli E, Riccò S, de la Torre A, Walker S M, Bruno F Y, King P D C, Meevasana W, Shi M, Radović M, Plumb N C, Gibbs A S, Mackenzie A P, Berthod C, Strand H U R, Kim M, Georges A and Baumberger F 2019 *Phys. Rev. X* **9** 021048